 CMC, vol.41, no.2, pp.85-110, 2014

Analysis on Flexural Behavior of UHPFRC Beams based on Tensile Stress-Crack Opening Relationship

Jung Soo Lee[1], Sung Yong Park[2], Keunhee Cho[2], Jeong-Rae Cho[2] and Seung Hee Kwon[1,3]

Abstract: The objective of this study is to investigate the differences between the tensile stress-crack opening relationships of the small size notched beam and the real size beam which were made of two ultra-high performance fiber reinforced concretes (UHPFRCs) having different volume fractions and lengths of fibers. The stress-crack opening relationships of two UHPFRCs were first obtained from the inverse analysis for the small size notched beam tests. In addition, the three types of real size beams were manufactured for each mix: (1) plain beam, (2) beam with tensile reinforcement, and (3) beam with both tensile and compressive reinforcements. The flexural tests of the plain and reinforced beams were conducted up to a failure state. The load-deflection curves of the plain and reinforced UHPFRC beams calculated based on the tensile stress-crack opening relationship of the notched beams did not give an accurate prediction on the measured load-deflection curves of the real size beams. The tensile stress-crack relationships accurately fitting the measured load-deflection curves were additionally found, and the difference in the tensile stress-crack opening relationships of the small size notched beams and the real size beams was analyzed in this study.

Keywords: UHPFRC, flexural behavior, cracking, fracture, tensile stress-crack relationship.

1 Introduction

The outstanding mechanical properties of Ultra High Performance Fiber Reinforced Concrete (UHPFRC) have been revealed in numerous studies [Reda et al.

[1] Department of Civil and Environmental Engineering, Myongji University, Korea, Yongin, South Korea.
[2] Korea Institute of Construction Technology, 2311, Daehwa-dong, Goyang 411-702, South Korea.
[3] Corresponding author. Tel.: +82 (31) 330-6418; Fax: +82 (31) 336-9705; Email: k-won08@mju.ac.kr

(1999); Kang et al. (2010); Kim et al. (2011); Yang et al. (2011); Kang et al. (2011)]. The disuse of coarse aggregates for the optimization of granular mixtures in UHPFRC leads to a homogenous and dense cementitious matrix that demonstrates ultra-high compressive strength and tensile strength of more than 150MPa and 10MPa, respectively [Richard and Cheyrezy (1995); Charron et al. (2004); Habel et al. (2006)]. The fiber contained in UHPFRC plays a critical role in enhancing the ductility for tensile cracking, and the ultimate tensile strain capacity was reported to be up to 5x10^{-3} [Rossi et al. (2005)]. UHPFRC also has very high durability due to the low permeability of its dense matrix [Kang et al. (2010)]. Based on the excellent mechanical properties and durability, it is expected that UHPFRC will be widely applied to real structures or structural members in the near future.

The flexural member is one of the most potential structural elements that UHPFRC is expected to be applied to soon because its high strength in compression and tension, and high ductility certainly enhance the structural performances of beams [Yang et al. (2010)]. Differently from the design of the ordinary reinforced concrete beams, the contribution of the cracking resistance, namely, the softening relationship between the tensile stress and cracking opening, to the flexural behavior of the UHPFRC beams should be taken into account. The softening relationship is generally obtained from fracture tests such as notched beam tests, wedge splitting tests, or direct tension tests with UHPFRC specimens of small size. Although the softening relationship experimentally determined from the small specimens is used in analyzing the flexural behaviors of UHPFRC beams of real scale, there is some limitation in accurately predicting the flexural behavior of the UHPFRC beams.

The tensile stress-crack opening relationship or the softening relationship of the cementitious material, namely, the matrix of fiber reinforced composites depends on a size of structure and a boundary condition and is not a material property but a structural property [Van Mier (2010); Kwon et al. (2008)]. In addition, the softening relationship for tensile cracking of UHPFRC highly also depends on the dispersion and orientation of fibers, which are also affected by beam size as well as the manufacturing process such as mixing and casting [Kang et al. (2011); Wille and Parra-Montesinos (2012)]. Therefore, the softening relationship obtained from the small laboratory tests cannot be applied to designing and predicting tensile cracking behavior of real size structures. Nevertheless, a most convenient and practical way to predict the real behavior of the structures is to apply the tensile softening relationship to an analytical or a numerical analysis. For this reason, it needs to find how much different the tensile softening relationship is according to the size.

The objective of this study is to investigate the differences between the softening relationships of the small size notched beam and the real size beam which was made of two UHPFRCs. Notched beam specimens of small size, 150mm x 150mm x 550mm, and plain and reinforced beams of 200mm x 250mm x 2,200mm were manufactured with two UHPFRCs having different volume fractions and lengths of fibers. The softening relationships for tensile cracking optimally fitting the load-CMOD curves measured from the fracture tests for the notched beam specimens were first found from the inverse analysis. The finite element analyses for the plain and the reinforced beams were performed with the softening relationship of the notched beams. The load-deflection curves calculated from the analyses were compared with the measured load-deflection curves, and the difference between them was estimated. The softening curves of the notched beams were modified to accurately fit the load-deflection curves. The difference between the original and the modified softening relationships were examined.

2 Experiments

2.1 Materials

The mix proportions of the two UHPFRCs are listed in Table 1. The water to binder ratio w/b was 0.2, and the dosage of silica fume was 25% of cement weight. In the first mix U1, 13 mm long fiber contained as much as 2.0% of the total volume. In the second mix U2, fibers of 16.3 mm and 19.5 mm in length were added into the mix in portions as high as 0.5% and 1.0%, respectively. The fiber was made of steel and had a straight shape. The diameter of all the fibers was 0.2 mm. The density and the yield strength of the fibers were 7,800 kg/m^3 and 2,500MPa, respectively. Fine aggregates with a density of 2,620 kg/m^3 and sand with a mean particle size below 0.5 mm were used. Polycarboxylate superplasticizer was added into the mixes in quantities as high as 1.8% of the cement weight. The use of filler through the partial replacement of cement generally provides faster strength gains at early age as well as durability. Siliceous filler with a mean particle size of 26.6 μm was applied.

Table 1: Mix Proportions

Mix	Steel Fiber		Relative weight ratio to cement					
	Length (mm)	Volume fraction (%)	Cement	Water	Silica fume	Fine aggregates	Filler	Superplasticizer
U1	13.0	2.0	1.00	0.25	0.25	1.10	0.30	0.018
U2	16.3	0.5						
	19.5	1.0						

In the mixing processes, cement, silicafume, filler, and fine aggregate were first premixed for approximately 10 minutes. Next, water and superplasticizer were added and mixed for another 10 minutes. After the mixture became flowable, the steel fibers were finally added and mixed for an additional 5 minutes.

2.2 Notched UHPFRC beam specimens

Fig. 1(a) shows the dimension of the notched beams. For each mix, three companion specimens were manufactured, and the dimension of the specimen was 150mm x 150mm x 550mm. After the UHPFRC was placed into the molds, the beams were cured under wet conditions at 20° for one day and then were demolded. After demolding, steam was conducted at $90 \pm 5°$ for 72 hours. The notch was made by diamond saw cutting, and the depth of the notch was 50mm.

Threepoint bend tests were performed as shown in Fig. 1(b). The COD (Clip On Displacement) gage was attached at the bottom to measure the CMOD (Crack Mouth Opening Displacement) as depicted in Fig. 1(c). The actuator was controlled by a constant displacement rate of 0.003 mm/sec. The applied load was measured by a 100 kN capacity load cell. The cylinder specimens of ϕ 100 mm x 200 mm were manufactured, and the compressive strength and elastic modulus were measured with them.

2.3 Plain and Reinforced UHPFRC Beams

As listed in Table 2, three different cases according to the reinforcement methods were considered in the experimental program: the first case (R0) is for plain beam with no reinforcement, the second (R2) is that the tension region was reinforced with two rebars, the third (R4) is that the tension and the compression regions were reinforced with two rebars.

The nominal diameter and cross-sectional area of the rebar were 15.9 mm and 198.6 mm^2, respectively. The yield stress of the rebar was 400 MPa. All the beams have the same dimensions, 200 mm(width) x 250 mm(height) x 2,200 mm(length).

A metallic form was first installed. Then, the rebar was arranged. All the beams were cast with the UHPFRC, which came from the same batch used in manufacturing the notched beam specimens, and the same curing process was applied to the plain and reinforced beams. Fig. 2 illustrates the manufacturing process of the beam specimens.

The strain gages to measure the strain at the top, side, and bottom faces were attached as shown in Fig. 3(a). The displacement gages were also installed to measure the deflections at the middle and the quarter positions of the beams. Four-point bend tests were performed. The spacing of the load points was 500 mm. The actua-

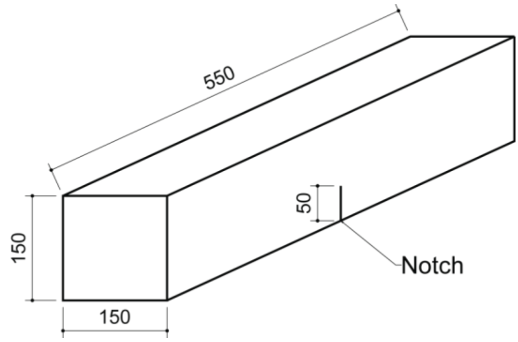

(a) Dimension of notched beam specimen (unit:mm)

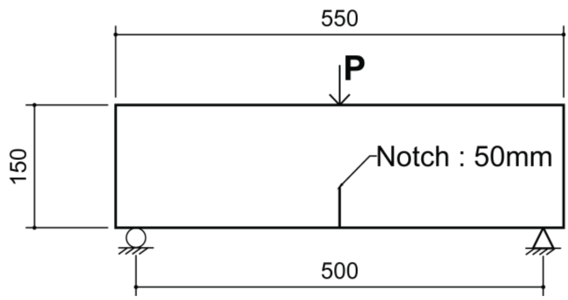

(b) Tree-point bend test(unit:mm)

(c) Installation of COD gage

Figure 1: Notched specimen and test setup.

tor was controlled by a constant displacement rate of 0.01 mm/sec, and the applied load was measured with a 1,000 kN capacity load cell. Fig. 3(b) shows the real test setup.

Table 2: Test program for UHPFRC beams.

Specimen	R0	R2	R4
Cross section	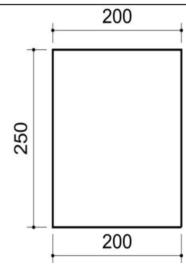	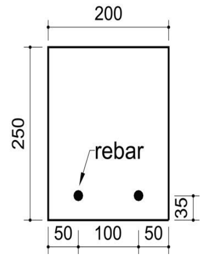	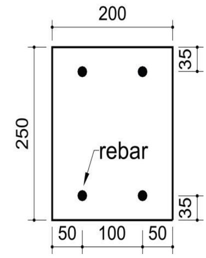
Rebar	-	2-D16	4-D16
Rebar ratio	-	0.0079	0.0159
UHPFRC	U1, U2	U1, U2	U1, U2
The Number of Companion Specimens	2	2	2

3 Softening Relationship for Tensile Cracking

3.1 Data processing

The load-CMOD curves measured from the three companion notched beam specimens for each mix were averaged in the method proposed by an existing study (Zhao et al. 2008, Kwon et al. 2008). There are several steps in the averaging method. First, the data scattered far from the load-CMOD curve are filtered, and one point is taken every 20 points along the load-CMOD curve (Fig. 4(a)). Second, an average is taken of five points consisting of the given point in the first step and two points above and below the given point. Third, 100 equally-spaced CMOD values are calculated from the zero point to the CMOD at the peak load point, and another 100 CMOD values are calculated from the peak to the end point. The end point of the CMOD for each specimen is set such that the distance from the peak to the end point is identical for the two companion specimens. Fourth, the load values corresponding to the 100 CMOD values are calculated by interpolation between the averaged data points for the ascending and descending parts (Fig. 4(b)). Finally, the 200 CMOD values and the corresponding load values for each companion are averaged in the order sequenced (Fig. 4(c)).

According to the equivalent elastic crack approach based on the Griffith–Irwin

(a) Preparation of form

(b) Pouring UHPFRC into the form

(c) Finish work

Figure 2: Manufacturing process of UHPFRC beams.

cracking mechanism (Bazant and Kazemi), the fracture process zone (FPZ) is formed with an increase of the applied load, and the equivalent extension of the crack length, which is elastically equivalent to the process zone, is largest at the peak. After the peak load, the process zone starts to move forward along the crack path, maintaining the largest equivalent extension size. When averaging the test data between the companions, each averaging point of the data has to represent the same fracture status. The 100th data point represents the peak load status for each specimen, and is in the same fracture status. For each of the equally spaced 100 CMODs up to the peak and the corresponding loads, the ith data point for each specimen can be assumed to be in the same status, namely, the *i*th step of increasing the fracture process zone. The end points (200th data points) of the descending part represent the same status that the largest equivalent extension is moved the same

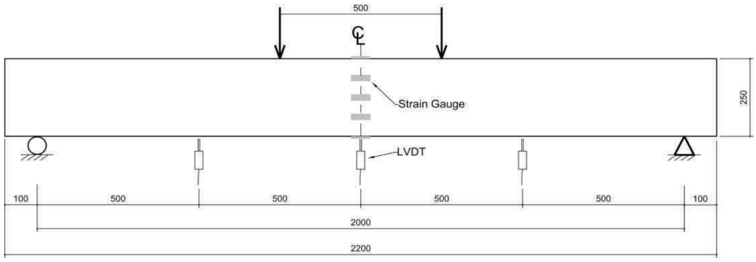

(a) Installation of gages

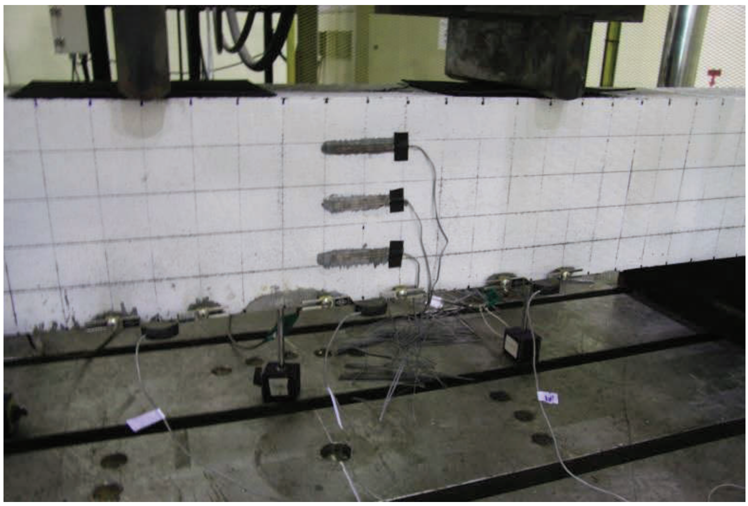

(b) Test setup

Figure 3: Gage installation and test setup of UHPFRC beams.

distance from the peak point. The *i*th data point in the descending region can also be considered as the same status that the fracture process zone is equally far from the peak, because each data point is equally spaced. For this reason, 200 equally spaced CMOD values and the corresponding load values for each specimen can be averaged.

In order to find the softening curve that optimally fits the load-CMOD curves, an inverse analysis was conducted. Because the number of data points used in the optimal fit of the inverse analysis significantly affects computer running time, the minimum number of data points representing the load-CMOD curve is desirable. From the averaged data for the companion specimens, the minimum number of data points was extracted according to the method proposed in the previous study (Zhao et al. 2008, Kwon et al. 2008). Six points and twelve points were found for the ascending and descending parts, respectively (Fig. 4(d)).

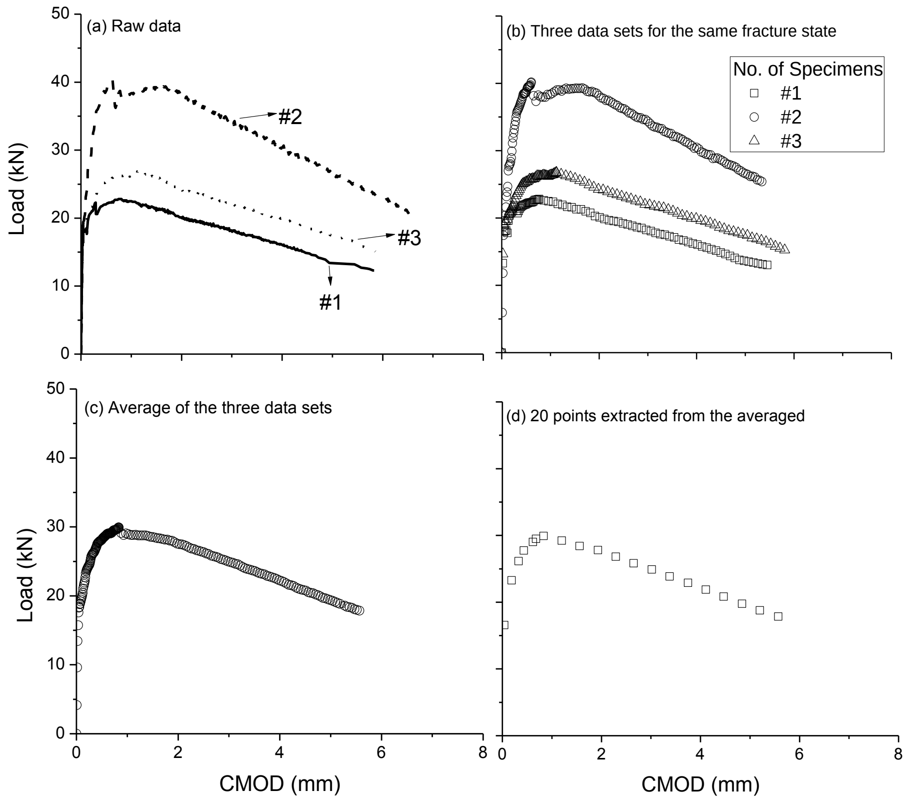

Figure 4: Data processing for three companion notched beam specimens (Mix U1).

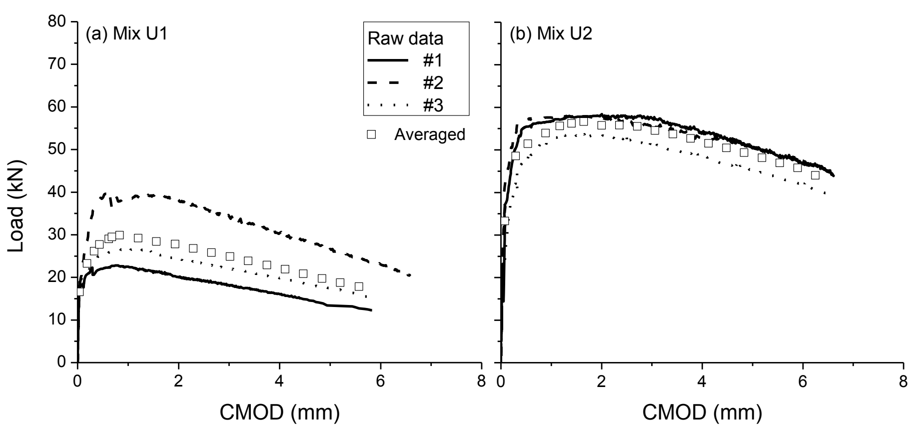

Figure 5: Measured and Averaged Load-CMOD relationships.

Fig. 5 shows the load-CMOD curves measured from three companion specimens for the mixes, U1 and U2, and the averaged curves that will be used in the inverse analysis. In Fig. 5(a), a sudden load reduction near the peak load was observed in the specimens U1-#1 and U1-#2. The sudden reduction seems not a general characteristic of the mix U1but a small variation due to the inhomogeneity in the dispersion and the orientation of the fiber. The averaged load-CMOD curve of Fig. 5 (a) demonstrates that the effect of the sudden reduction is minor.

3.2 Inverse Analysis

There are several methods to obtain the relationship between the tensile stress and crack opening (Rilem TC-198 2007). In this study, the inverse analysis based on the optimization process and the finite element method was chosen to obtain the relationships of the notched beam specimens. There were several shapes of the relationship proposed and employed in the literature (Rilem TC-198 2007, Kang et al. 2008). The shape has to be determined before the inverse analysis. There may be a problem that the relationships with different shapes can fit the test data with a similar accuracy. If the shape is highly nonlinear and unnecessarily consists of many parameters, some of the parameters would be very sensitive to the test data and the determined values of the parameters would not be physically meaningless. Therefore, a simple shape that can accurately fit the test data was selected in this study.

The relationship depends on the type of fibers and the mechanical properties of the matrix. The relationship usually consists of two parts: the strain hardening occurs first and the strain softening is followed. However, the strain hardening region may be is too small to be ignored in some UHPFRCs. The existing design recommendations (SETRA/AFGC 2002, JSCE 2007) also suggest both the strain hardening and the strain softening relationships between the tensile stress and crack opening. It was found from the previous studies (Kang et al. 2008, Kang et al. 2010) that the bilinear softening curve of Fig. 6 (a) can be used in designing of the UHPFRC similar to the mixes used in this study. In the inverse analysis, the bilinear strain softening curve of Fig. 6(a) was used to fit the load-CMOD curves.

Fig. 7(a) shows the algorithm of the inverse analysis, in which finite element analysis is repeatedly performed, reassuming the parameters of the softening curve until the error between the measured and calculated load-CMOD curves is less than a given tolerance (Kwon et al. 2008). The Marquardt-Levenberg method (Brown 1970) was used in the optimization. Fig. 7(b) is the finite element mesh refinement for the wedge-splitting specimen. Only half of the specimen was modeled considering its symmetry. The total number of elements and the number of nodes on the ligament were 836 and 35, respectively.

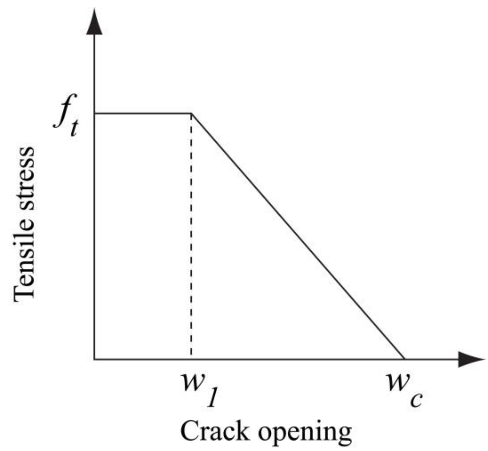

(a) Softening curve for the notched beam specimen

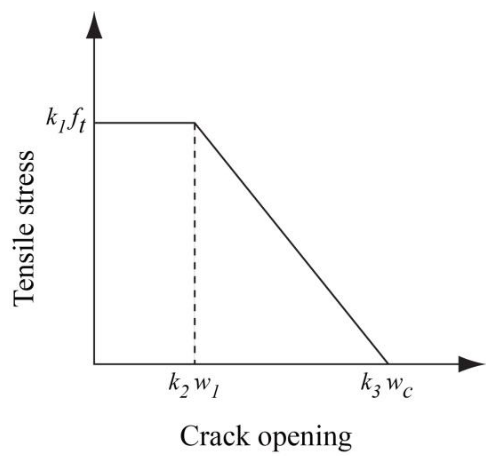

(b) Modified softening curve for the real size beam

Figure 6: Bilinear softening curve.

3.3 Softening curve of the notched beams

Fig. 8 is a comparison between the measured load-CMOD and the calculated load-CMOD based on the softening curve obtained from the inverse analysis. It can be seen that the softening curve accurately simulates the real load-CMOD curve, and the usage of the bilinear softening curve was appropriate for the UHPFRC used in this study. The parameters of the softening curve, the measured compressive strength, the elastic modulus, the modulus of rupture, and the limit of proportion-

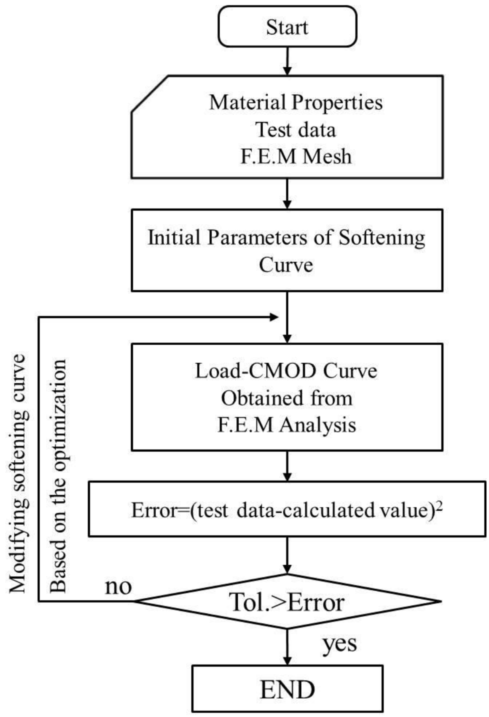

(a) Algorithm

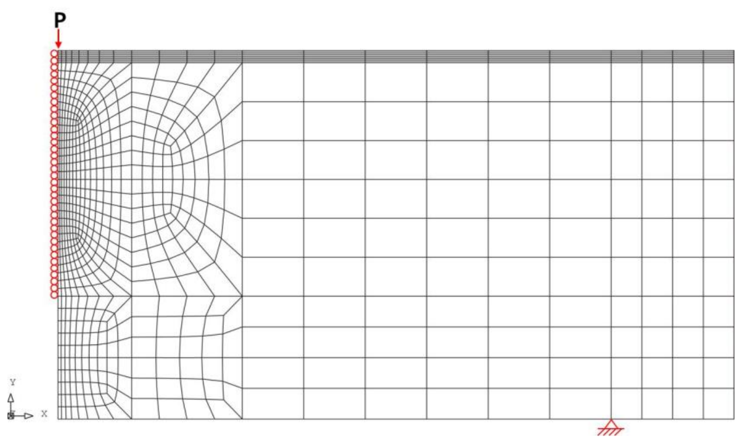

(b) Finite element mesh for notched beam specimen

Figure 7: Algorithm and finite element mesh employed in inverse analysis.

ality are listed in Table 3. The fracture energy is the area of the softening curve and is also included in Table 3.

The fracture energy of the Mix U2 is almost three times higher than that of the Mix U1. The Mix U2 contains longer fibers than does the Mix U1, as shown in Table 1, and the larger bridging effect of the longer fiber may result in higher fracture energy. The softening curve of the notched beams will be used in analyzing the flexural behavior of the plain and reinforced UHPFRC beams.

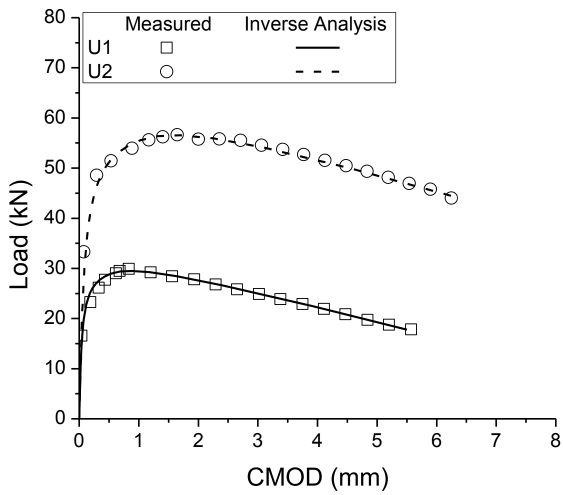

Figure 8: Comparison between the measured load-CMOD and the load-CMOD obtained from the best fits.

Table 3: Prameters of the optimized softening curve and other mechanical properties.

Mix	Softening Curve			Compressive Strength (MPa)	Elastic Modulus (GPa)	Fracture Energy (N/mm)	Modulus of rupture (MPa)	Limit of Proportionality (MPa)
	f_t (M-Pa)	w_1 (m-m)	w_c (m-m)					
U1	5.45	0.30	5.02	160	51	14.5	4.32	3.36
U2	10.4	0.60	8.30	203	56	46.3	8.19	7.02

4 Numerical Analysis for Plain and Reinforced UHPFRC Beams

4.1 General

In order to examine how accurately the softening curves of the notched beams can predict the flexural behavior of the plan and reinforced UHPFRC beams, finite element analyses for the beam specimens were performed. A comparison between the test and analysis results for the load-deflection curves was made, and some important results also were obtained from the analyses. Fig. 9(a) shows the finite element mesh for the beam specimens. Half of the beam was modeled considering the symmetry of the beam. The four node plane element was used for modeling concrete, and the embedded element was employed for modeling rebar. The commercial program DIANA Ver. 9.1 was used in the finite element analysis. The material models for tensile cracking used in this study are not provided by the program, and specially coded subroutines for the models were incorporated into the program.

4.2 Modeling of UHPFRC

The tensile cracking was modeled as the crack band model [Bazant and Oh (1983)]. Because every element must have an identical fracture energy, the crack opening of the softening curve is transformed into the cracking strain of the continuum body by dividing the displacement by the crack band width, as shown in Fig. 9(a). All the four node elements were square having the same size. The one side of the element was 5.0 mm which is the crack band width. The crack direction was determined based on the direction of the principal stresses in the numerical calculation. The softening curve of Table 3 was used for simulating the tensile cracking of the UHPFRC beams.

In order to simulate the multiple cracking in the beams, the modeling method used in the existing study [Kwon and Shah (2008)] was employed in this analysis. In the modeling UHPFRC, the tensile strength was randomly distributed and was assumed to be more than 98% and less than 102% of the reference tensile strength , f_t, given in Table 3. Fig. 9(b) shows an analysis result for the beam. The highlighted parts in the figure are the tensile cracks, namely, the multiple cracking.

Fig. 10 shows the measured stress and strain under compression for mixes U1 and U2. Based on the test results, it was assumed that the stress and the strain have a linear elastic relationship up to the ultimate stress level and the failure happens right after the strain exceeding the strain at the strength. The elastic modulus and compressive strength listed in Table 3 were used in the analysis. In the softening curve, unloading and reloading paths were specified as the same path that is heading for the origin point, as shown in Fig. 11.

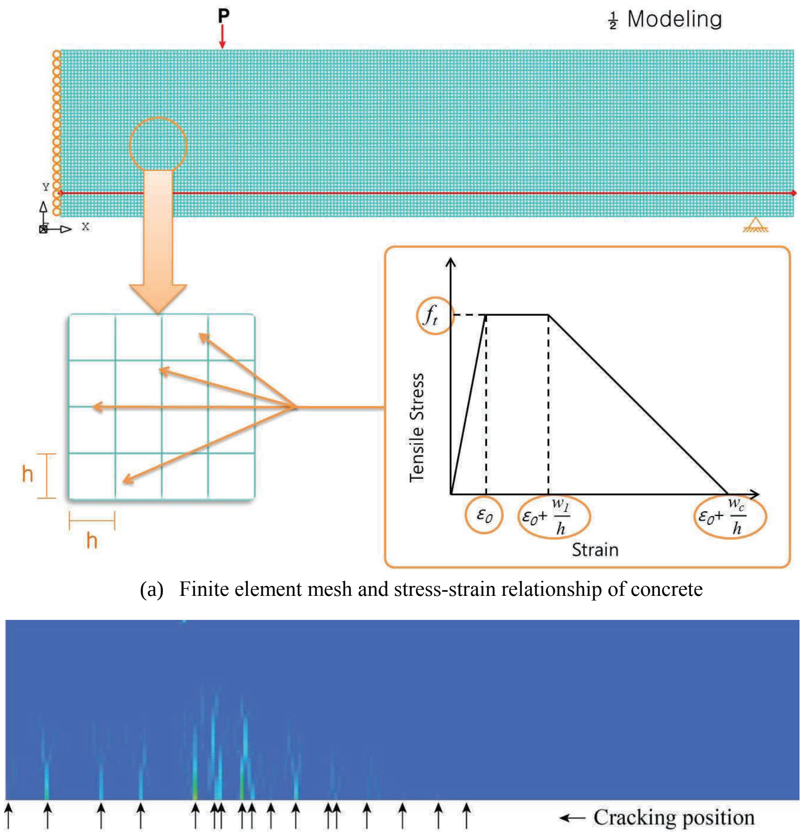

(a) Finite element mesh and stress-strain relationship of concrete

(b) Multiple cracking considered in the modeling

Figure 9: Finite element modeling for UHPFRC beam.

4.3 Modeling of rebar

As for the rebar, the linear elastic relationship was assumed up to the yield stress of 400 MPa , and the perfect plastic was considered after the yield stress. The elastic modulus and Poisson's ratio of the rebar were 200GPa and 0.3, respectively. A perfect bond between the rebar and the UHPFRC was assumed. A tensile test for the rebar was not conducted in this study. The actual yield stress for the rebar used in the test has been reported to be 5 % to 10 % higher than the nominal yield stress of 400 MPa [Kook et al. (2010); Hwang et al. (2011)]. In the flexural behavior of the beam, the slight difference in the yield stress may not greatly alter the load-deflection relationship of the beam because the yield strain of the rebar is localized at the crack and the rebar is in the elastic state in the region beside the crack.

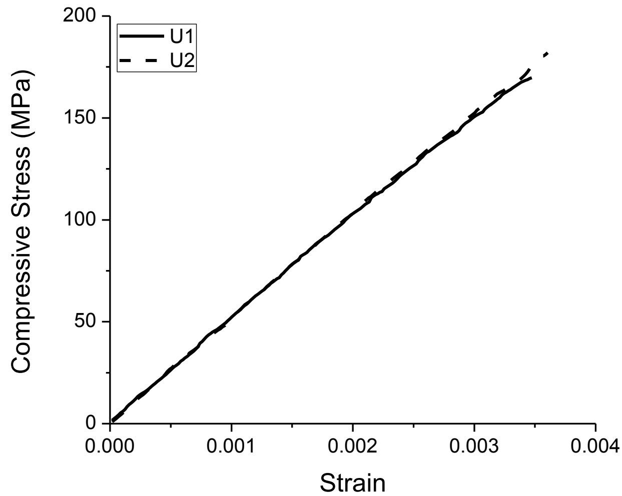

Figure 10: Compressive stress-strain curve.

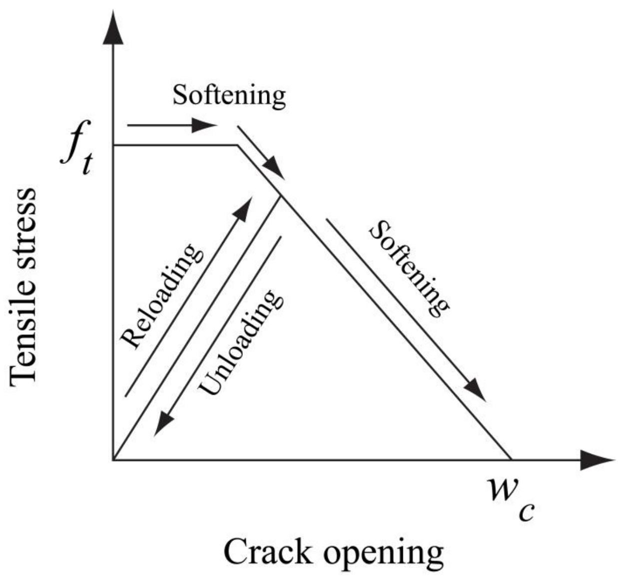

Figure 11: Loading paths in the softening curve.

5 Test and Analysis Results

5.1 Test results

Fig. 12 shows the load-strain relationship measured from the second companion specimen of U2-R2. In every graph of this paper, the load means the total force applied to the specimen. The strain measured on the top surface at the peak load is -2,200 x 10^{-6}, which is smaller than the ultimate strain of UHPRFC material at the compressive strength, as can be seen in Fig. 10. It indicates the peak load was governed by the tensile cracking and yielding of the reinforcement. The strain measured at the upper position over the side surface is in compression under the load of 200 kN and changes into tension after the load level. It means that the neutral axis of the beam suddenly went up after the load level, probably because the reinforcement starts to yield at a load of 200kN. All the strains also abruptly increased after yielding of the reinforcement. The strain measured on the bottom surface exhibits the largest tensile values because a crack initiates from the bottom, and its width increases with the increase of the applied load. The increasing rate of the strains slightly changes at the load of 85 kN, at which the macro crack seems to initiate. The stains measured from all the specimens behaved similarly to the results of Fig. 12.

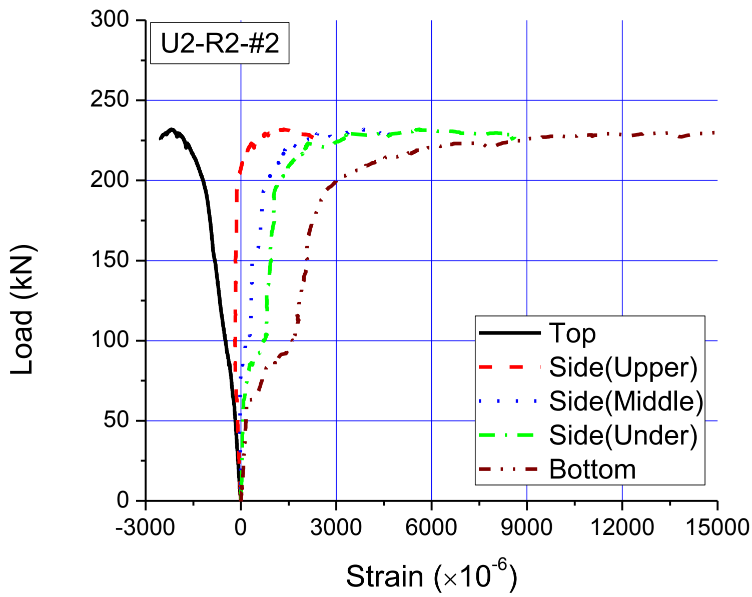

Figure 12: Typical load-strain curve (U2-R2-#2).

Fig. 13 is the load-deflection curve measured from the same specimen as in Fig. 12. The solid line is the deflection measured at the center of the specimen, and the dashed and dotted lines are the measured deflections at the quarter positions of the beam, as shown in Fig. 3(b). At the cracking load, 85 kN, the initial steep linear relationship changes. The load increases with a lower rate up to the yielding point of reinforcement, 200 kN. After that, the deflection gently increases up to the peak. The deflection at the mid-span is the largest, and the deflections at the two quarter positions are almost identical due to the geometric symmetry. Fig. 13 also exhibits a typical load-deflection curve for all the specimens.

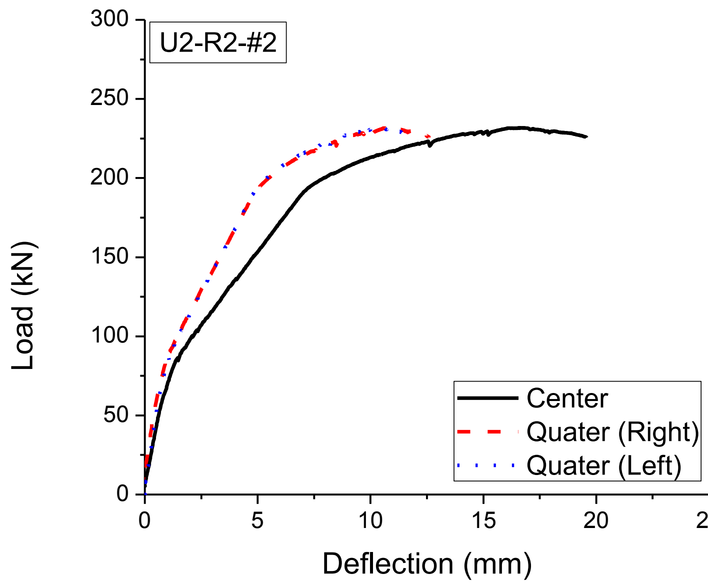

Figure 13: Typical load-deflection curve (U2-R2).

The two companion specimens for each case of Table 2 were tested. The load-deflection curves measured at the mid-span of the two companion specimens were averaged in a similar manner to the method explained in the Subsection 3.1. The averaged load-deflection curves are plotted in Fig. 14, and the peak load and the deflection at the peak load are listed in Table 4 based on the results of Fig. 14. The peak loads and the deflections at the peak loads for the Mix U2 are larger than those for the Mix U1 except for one case, U1-R0. It may be attributed to the fact that the cracking resistance of the Mix U2 is larger than that of the Mix U1, as previously explained in Table 3. However, it is necessary to quantitatively estimate the effect of the softening relationship for the tensile cracking on the load-deflection curves, namely, the flexural behavior of the UHPFRC beams.

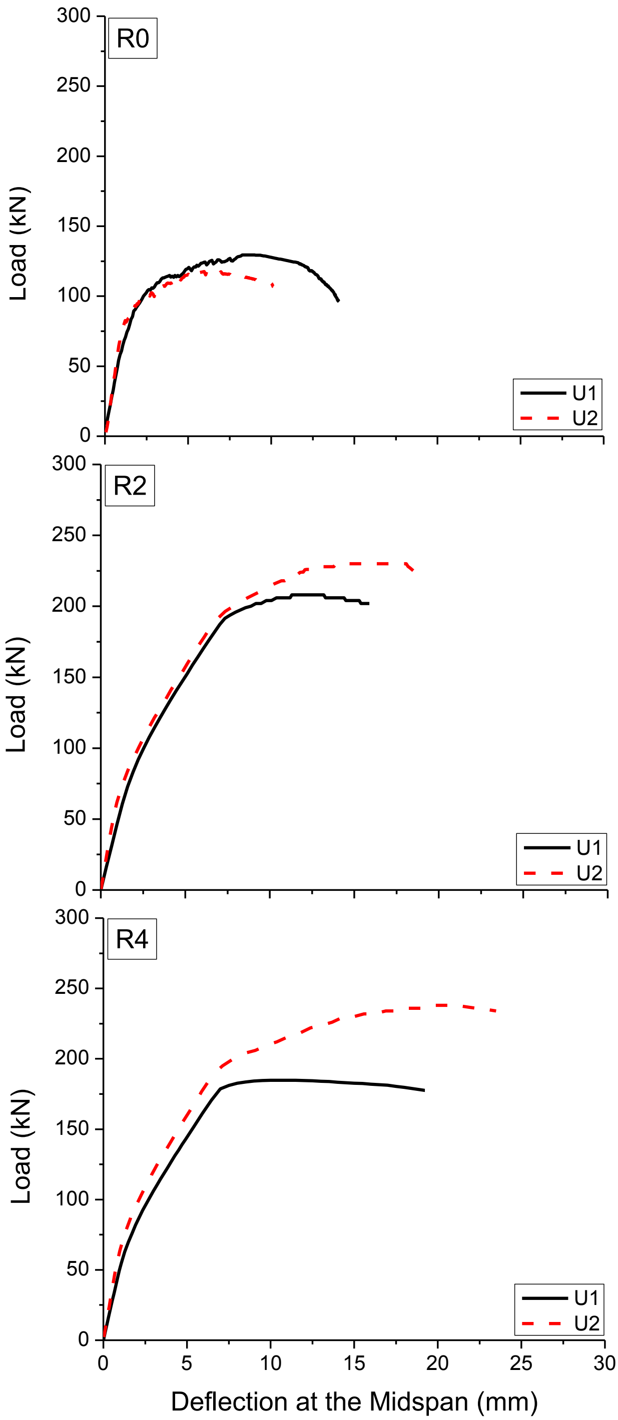

Figure 14: Load-deflection curves measured at the mid-span.

5.2 Comparison between the measured and the calculated load-deflection curves

The load-deflection curves were calculated through the numerical analyses explained above, and the calculated curves are compared with the measured curves in Fig. 15. The dashed lines are the curves calculated based on the softening curves of the notched beams of Table 3, and the square dots are the measured curves. In the case of the Mix U1, the calculated load-deflection curves are lower than the measured one. Contrarily, the calculated curves are higher than those measured in the Mix U2.

Based on the results of Fig. 5 that the load-CMOD curve of the Mix U1 is lower than that of the Mix U2, it was expected that the load-deflection curve of U1-RO is lower than that of U2-R0. However, the load- deflection curves of U1-R0 and U2-R0 were very similar to each other as shown in Fig. 14, which is due to the fact that the measured curves of U1-R0 and U2-R0 were higher and the lower than the expected curves (the dashed lines), respectively, as depicted in Fig. 15.

The peak loads and the deflections of the calculated curve are also listed in Table 4. The values in the parenthesis in the table are the error between the measured and the calculated curves. The error is the ratio of the difference between the measured and the calculated to the measured. The error for the peak loads range from 3.4% to 36.2%, and the error for the deflections range from 3.5% to 67.7%. Except two cases, U1-R2 and U1-R4, the softening curves obtained from the notched beam tests do not give accurate predictions for the real flexural behavior of the UHPFRC beams. This is because the fiber dispersion and orientation of the notched beam specimen are different from those of the UHPFRC beams. It is necessary to find softening curves that fit the load-deflection curves and to examine the difference between the softening curves of the notched beams and the softening curves capable of fitting the load-deflection curves.

5.3 Modified softening curves optimally fitting the measured load-deflection curves

The softening curves were modified to fit the measured load-deflection curves. Factors altering the parameters (f_t, w_1, and w_c) of the softening curve of Fig. 5 (a), k_1, k_2, and k_3, were introduced, as shown in Fig. 5 (b). By adjusting the factors and repeatedly performing the numerical analyses for the UHPFRC beams, the best fits for the load-deflection curves were found in a heuristic manner. The load-deflection curves calculated based on the modified softening curves (MSC) were compared with the measured in Fig. 15 as well. Although the fits may not be optimal, the fits accurately simulate the real flexural behavior, and the modified softening curves are at least very close to optimal ones. In Table 4, the peak loads and the deflections at

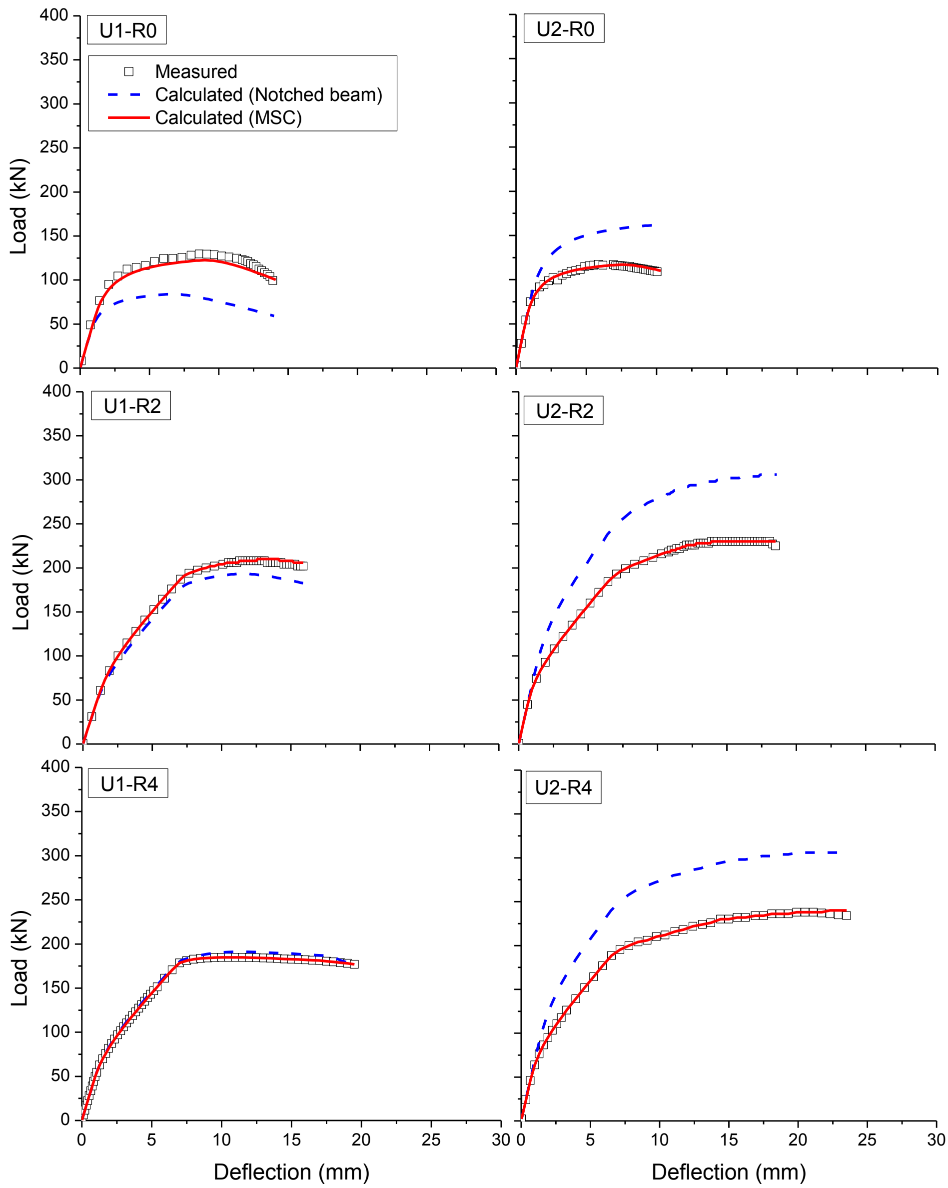

Figure 15: Comparison between the measured and the calculated load-deflection curves at the mid-span.

the peak loads obtained from the modified softening curves are included, and the error is also listed.

The found k factors are listed in Table 5. For the Mix U1, k_1 ranges from 0.965 to 1.47, k_2 from 0.850 to 1.33, and k_3 from 0.850 to 1.20. The averaged k factors are all more than 1.0, which means that every parameter of the softening curve of the notched beam for the Mix U1 needs to be magnified to fit the real load-deflection curves of the UHPFRC beams. Differently from the Mix U1, the $k$factors are all less than 1.0 except one case for k_3 of U2-R4. The softening curves of the notched beams and the softening curves based on the averaged k factors were compared in Fig. 16. The comparison indicates that the softening curve of the notched beam for the Mix U2 needs to be demagnified to fit the real load-deflection curves of the UHPFRC beams. The difference between the softening curve of the notched beam and the modified softening curve is larger in the Mix U2. As a result, the shorter fiber (13mm) of the Mix U1 is more dispersed and better oriented to the longitudinal axis in the process of manufacturing the real scale UHPFRC beams than in the manufacturing the small size specimens. Contrarily, the dispersion and the orientation of the longer fibers (16.3mm and 19.5mm) become worse in the UHPFRC beams than in the small size notched beams.

Table 4: Peak loads and deflections at the peak load.

<table>
<tr><th rowspan="3">Mix</th><th rowspan="3">Reinforcement</th><th colspan="3">Peak Load (kN)</th><th colspan="3">Deflection at the peak load (mm)</th></tr>
<tr><th rowspan="2">Measured</th><th colspan="2">Calculated</th><th rowspan="2">Measured</th><th colspan="2">Calculated</th></tr>
<tr><th>Notched beam</th><th>MSC</th><th>Notched beam</th><th>MSC</th></tr>
<tr><td rowspan="3">U1</td><td>RO</td><td>129</td><td>84
(35.1%)</td><td>123
(5.3%)</td><td>8.26</td><td>6.89
(16.6%)</td><td>8.99
(8.8%)</td></tr>
<tr><td>R2</td><td>208</td><td>193
(7.0%)</td><td>210
(1.0%)</td><td>13.2</td><td>11.8
(10.6%)</td><td>14.1
(6.8%)</td></tr>
<tr><td>R4</td><td>184</td><td>191
(3.4%)</td><td>185
(0.0%)</td><td>11.5</td><td>11.9
(3.5%)</td><td>11.5
(0.0%)</td></tr>
<tr><td rowspan="3">U2</td><td>R0</td><td>119</td><td>163
(36.2%)</td><td>117
(2%)</td><td>6.44</td><td>10.8
(67.7%)</td><td>7.11
(10.4%)</td></tr>
<tr><td>R2</td><td>230</td><td>306
(33.0%)</td><td>230
(0.0%)</td><td>18.1</td><td>19.1
(5.5%)</td><td>18.6
(2.8%)</td></tr>
<tr><td>R4</td><td>238</td><td>306
(28.6%)</td><td>240
(0.8%)</td><td>21.1</td><td>24.7
(17.1%)</td><td>23.5
(11.4%)</td></tr>
<tr><td colspan="8">The values in the parenthesis are errors between the measured and the calculated values.</td></tr>
</table>

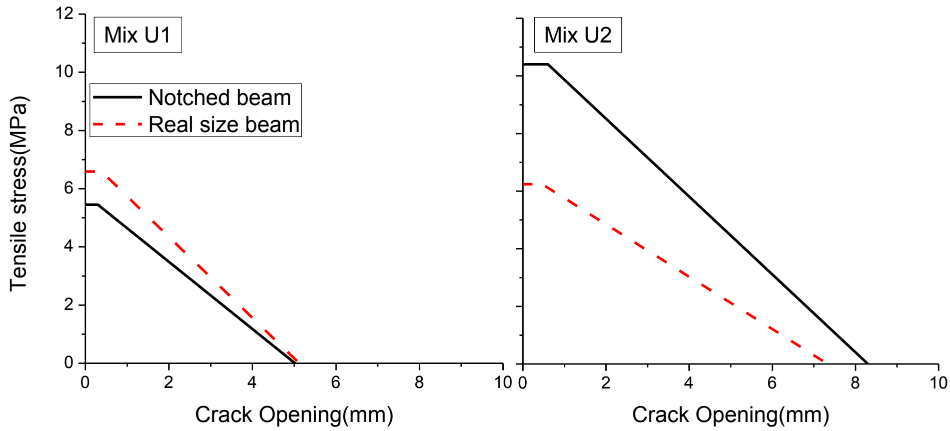

Figure 16: Comparison of the softening curves for the notched beam and the real size beam.

When designing HHPFRC beams as a real structural member, the softening curve for tensile cracking should be taken into account in calculating the peak loads and the deflections at the peak loads. The softening curve is generally determined from the small size tensile fracture tests. However, the softening curve found from small size specimens may not give an accurate prediction for the flexural behavior. The k factors given in Table 5 may not be directly used in practical design because the scope of this study is limited to develop a general model on the softening curve applied to the real size structural member. However, the results of Table 5 provides useful information on how much the softening curves found from the fracture tests of small specimens can vary in the real size UHPFC beams.

Table 5: k-factors of the modified softening curves.

Mix	Reinforcement	k-factors			Averaged k-factors		
		k_1	k_2	k_3	k_1	k_2	k_3
U1	RO	1.47	1.33	1.00	1.21	1.28	1.02
	R2	1.18	1.67	1.20			
	R4	0.965	0.850	0.850			
U2	R0	0.719	0.667	0.725	0.600	0.778	0.883
	R2	0.529	0.833	0.725			
	R4	0.550	0.833	1.20			

6 Conclusions

From this study, the following conclusions can be drawn.

1. UHPFRC containing 0.5% volume fraction of 16.3 mm fiber and 1.0% volume fraction of 19.5 mm fiber (the Mix U2) has higher cracking resistance due to the larger bridging effect of the longer fiber compared to UHPFR containing a 2.0% volume fraction of 13.0 mm fiber (the Mix U1).

2. The peak loads and the deflections at the peak loads for the Mix U2 are larger than those for the Mix U1. This may be attributed to the fact that the cracking resistance of the Mix U2 is larger than that of the Mix U1

3. The tensile stress-crack relationships obtained from inverse analyses for the notched beam tests of small size do not give an accurate prediction for the peak loads and the deflections at the peak loads of plain and reinforced UHPFRC beams of real scale. The maximum error for the peak loads was 36.2%, and the maximum error for the deflections at the peak loads was 67.7%.

4. The shorter fiber (13 mm) of the Mix U1 is more dispersed and better oriented to the longitudinal axis in the process of manufacturing the real scale UHPFRC beams than in the manufacturing the small size specimens. Contrarily, the dispersion and the orientation of the longer fibers (16.3 mm and 19.5 mm) become worse in the UHPFRC beams than in the small size notched beams.

5. The difference between the tensile stress-crack opening relationships obtained from the inverse analyses for the notched beams of small size and the tensile stress-crack opening relationships accurately fitting the load-deflection curves of the plain and the reinforced beams was examined. The analysis result on the difference provides useful information on how much the softening curves found from the fracture tests of small specimens can vary in the real size UHPFC beams.

Acknowledgement: This research was supported by a grant(13SCIPA02) from Smart Civil Infrastructure Research Program funded by Ministry of Land, Infrastructure and Transport(MOLIT) of Korea government and Korea Agency for Infrastructure Technology Advancement(KAIA). This paper was written in the sabbatical year of the fifth author. The fifth author is grateful for the support of Myongji University.

References

Bazant, Z. P.; Oh, B. H. (1983): Crack band theory for fracture of concrete. *Materials and Structures*, vol. 16, no. 93, pp. 155-177.

Baznat, Z. P.; Kazemi, M. T. (1990): Determination of fracture energy, process zone length and brittleness number form size effect with application to rock and concrete. *International Journal of Fracture*, vol. 44, pp. 111-131.

Brown, K. M. (1970): Derivative-free analogues of the levenberg, Marquardt and Gauss Algorithms for Non-linear Least Square Approximations. *IBM, Philadelphia Scientific Center Technical Report*, no. 320–2994.

Charron, J. P.; Denarie, E.; Brünhwiler, E. (2004): Permeability of UHPFRC under high stresses. *Proceedings of RILEM Symposium, Advances in Concrete through Science and Engineering, Evanston, Il. U.S.A.; March 2004*, pp.12.

Habel, K.; Viviani, M.; Denarie, E.; Brünhwiler, E. (2006): Development of the mechanical properties of an ultra-high performance fiber reinforced concrete (UHPFRC). *Cement and Concrete Research*, vol. 36, no. 7, pp. 1362-1370.

Hwang, H. J.; Park, H. G.; Choi, W. S.; Chung, L.; Kim J. K. (2011): Seismic performance of beam-column connections for special moment frame using 600 MPa flexural reinforcement. *Journal the Korea Concrete Institute*, vol. 23, no. 5, pp. 591-601. (in Korean)

JSCE. (2004): Recommendations for design and construction of ultra high-strength fiber-reinforced concrete structures.

Kang, S. T.; Joh, C.; Park, J. S.; Park, J. J.; Ryu, G. S.; Kim, B. S. (2008): The design guidelines for the tensile behavior of ultra-high performance concrete. *Proceedings of the Korea Concrete Institute*, vol. 24, no. 2, pp. 361-364. (in Korean)

Kang, S. T.; Lee, Y.; Park, Y. D.; Kim, J. K. (2010): Tensile fracture properties of an ultra high performance fiber reinforced concete (UHPFRC) with steel fiber. *Composite Structures*, vol. 92, pp. 61-71.

Kang, S. T.; Lee, B. Y.; Kim, J. K.; Kim, Y. Y. (2011): The effect of fiber distribution characteristics on the flexural strength of steel fiber-reinforced ultra high strength concrete. *Construction and Building Materials*, vol. 25, pp. 2450-2457.

Kim, D. J.; Park, S. H.; Ryu, G. S.; Koh, K. T. (2011): Comparative flexural behavior of hybrid ultra high performance fiber reinforced concrete with different macro fibers. *Construction and Building Materials*, vol. 25, pp. 4144-4155.

Kook, K. H.; Shin, H. O.; Kwahk, I. J.; Yoon, Y. S. (2010): Bond characteristics of ultra high performance concrete. *Journal of the Korea Concrete Institute*, vol.

22, no. 6, pp. 753-760. (in Korean)

Kwon, S. H.; Shah, S. P. (2008): Prediction of early-age cracking of fiber-reinforced concrete due to restrained shrinkage. *ACI Materials Journal*, vol. 105, no. 4, pp. 381-389.

Kwon, S. H.; Zhao, Z.; Shah, S. P. (2008): Effect of specimen size on fracture energy and softening curve of concrete: Part II. inverse analysis and softening curve. *Cement and Concrete Research*, vol. 38, no. 8-9, pp. 1061-1069.

Reda, M. M.; Shrive, N. G.; Gillott, J. E. (1999): Microstructural investigation of innovative UHPC. *Cement and Concrete Research*, vol. 29, no. 3, pp. 323-329.

Richard, P.; Cheyrezy, M. (1995): Composition of reactive powder concrete. *Cement and Concrete Research*, vol. 25., no. 7, pp. 1501-1511.

Rilem TC-198. (2007): Experimental determination of the stress-crack opening curve for concrete in tension. *Final Report 39*, pp. 39.

Rossi, P.; Arca, A.; Parant, E.; Fakhi, P. (2005): Bending and compressive behaviors of a new cement composite. *Cement and Concrete Research*, vol. 35, no. 1, pp. 27-33.

SETRA/AFGC. (2002): Ultra high performance fiber-reinforced concretes. *BFUP Groups.*

Van Mier, J. G. M. (2010): A fundamental explanation of softening. *Proceedings of the 7th International Conference on Fracture Mechanics of Concrete and Concrete Structures (FraMos-7), Jeju, Korea*, pp. 299-305.

Wille, K.; Parra-Montesinos, G. (2012): Effect of beam size, casting method, and support conditions on flexural behavior of ultra-high-performance fiber-reinforced concrete. *ACI Materials Journal*, vol. 109, no. 3, pp. 379-388.

Yang, I. H.; Joh, C.; Kim, B. S. (2010): Structural behavior of ultra high performance concrete beams subjected to bending. *Engineering Structures*, vol. 32, pp. 3478-3487.

Yang, I. H.; Joh, C.; Kim, B. S. (2011): Flexural strength of ultra high strength concrete beams reinforced with steel fiber. *Procedia Engineering*, vol. 14, pp. 793-796.

Yang, I. H.; Joh, C.; Kim, B. S. (2010): Structural behavior of ultra high performance concrete beams subjected to bending. *Engineering Structures*, vol. 32, pp.

Zhao, Z.; Kwon, S. H.; Shah, S. P. (2008): Effect of specimen size on fracture energy and softening curve of concrete: part I. experiments and fracture energy. *Cement and Concrete Research*, vol. 38, no. 8-9, pp. 1049-1060. 3478-3487.